

# NUMERICAL STUDY OF A HIGHLY UNDER-EXPANDED HYDROGEN JET

Xu, B.P., Zhang, J.P., Wen\*, J.X., Dembele, S. and Karwatzki, J.

School of Engineering, Kingston University  
Friars venue, Roehampton Vale, London, SW15 3DW, UK

## ABSTRACT

Numerical simulations are carried out for a highly under-expanded hydrogen jet resulting from an accidental release of high-pressure hydrogen into the atmospheric environment. The predictions are made using two independent CFD codes, namely CFX and KIVA. The KIVA code has been substantially modified by the present authors to enable large eddy simulation (LES). It employs a one-equation sub-grid scale (SGS) turbulence model, which solves the SGS kinetic energy equation to allow for more relaxed equilibrium requirement and to facilitate high fidelity LES calculations with relatively coarser grids. Instead of using the widely accepted pseudo-source approach, the complex shock structures resulting from the high under-expansion is numerically resolved in a small computational domain above the jet exit. The computed results are used as initial conditions for the subsequent hydrogen jet simulation. The predictions provide insight into the shock structure and the subsequent jet development. Such knowledge is valuable for studying the ignition characteristics of high-pressure hydrogen jets in the safety context.

**Keywords :** Hydrogen, under-expanded jet, Mach disk, large eddy simulation

## NOMENCLATURE

$C_p$	Specific heat, kJ/(kg-K)	$x, y, z$	Spatial coordinates, m
$D$	Diameter of orifice, m		
$G$	Filtering function	<b>Greeks</b>	
$H^{sgs}$	Sub-grid scale heat flux, kW/m <sup>2</sup>	$O$	Filter domain
$I$	Specific internal energy, J	$\rho$	Density, kg/m <sup>3</sup>
$J$	Heat flux vector	$\delta_{ij}$	Kronecker delta
$K^{sgs}$	Sub-grid scale turbulent kinetic energy	$\nu_t$	Sub-grid eddy viscosity
$P^{sgs}$	Production term	$\tau$	Viscous stress tensor
$P_r$	Turbulent Prandtl number	$\tau^{sgs}$	Sub-grid viscous stress tensor
$p$	Pressure, pa	$\rho^{sgs}$	Sub-grid scale mass flux
$Sc_t$	Schmidt number	$\tau^{sgs}$	Unresolved viscous work
$S_{ij}$	Strain rate tensor	$F^{sgs}$	Sub-grid species mass flux
$t$	Time. S	$\epsilon^{sgs}$	Dissipation term
$T$	Temperature, K	$\Delta$	Sub-grid length scale

---

\* Tel.: +(44)-208-547-7836

Email address: j.wen@kingston.ac.uk

## 1.0 INTRODUCTION

It is well known that the combustion of fossil fuels is responsible for the majority of the greenhouse gas emissions and a significant fraction of the air pollutant emissions in the world. The natural reserves of fossil fuels are also diminishing quickly. Hydrogen is one of the most promising substitutes of hydrocarbon-based fuels, due to the absence of carbon-based pollutants, the abundance of hydrogen in nature, and the ability to generate hydrogen from sustainable energy sources.

However, significant technical problems are associated with the storage of hydrogen because of its low density. In compressed gas systems operating at ambient temperature, the working pressures are in the region of 200–350 bar and potentially up to 700 bar. The Fuel cell vehicles (FCV) currently in trial use are mounted with hydrogen containers pressurized up to 400 bar and yield a driving range of 300–350 km per filling - roughly half of the gasoline vehicle's driving range. Industry is developing containers for up to 700 bar pressurization [16]. Accordingly there is an urgent need to study the safety implications of systems based on these very high pressures. As hydrogen has a wide flammability range (4–74% in air), the chance of ignition from any accident release is potentially much higher than common hydrocarbon fuels and this may give rise to slow deflagrations, fast deflagrations or under certain conditions detonations depending on the concentration, size of the cloud and the geometry involved.

This paper reports on the numerical simulation of an accidental release of a high-pressure round hydrogen jet into the open atmosphere. The flow of the hydrogen leak from a high-pressure tank is choked by the critical condition. Immediately downstream the leak, there exists a highly under-expanded shock structure, which is well-known from experiments [1-3]. As hydrogen leaks from the opening, it quickly expands and accelerates to a state of supersonic flow. The expansion waves originate around the expansion point, and where these meet the outer boundary of the hydrogen jet they are reflected as compression waves. The coalescence of these compression waves results in a barrel-shaped shock surrounding the immediate supersonic region and extending for a few diameters. High expansion of the jet also causes the pressure along the centreline to become so low relative to the ambient value that a recompression takes place through a characteristic normal shock (Mach disk). With respect to the highly under-expanded jet, the strength and width of the Mach disk are significant. Immediately downstream of the Mach disk, the flow is subsonic and the velocity is very low whilst the adjacent flow originating from the reflected shock is still supersonic. There exists a slip line at the boundary of these two concentric regions. These two streams quickly equilibrate their velocities leaving an approximately sonic flow. Due to the high strength of the Mach disk in highly under-expanded jet, only one Mach disk exists downstream the opening.

The existence of the complex shock structure and the very high velocity in the core of the barrel shock make the direct numerical simulation of the whole hydrogen jet region extremely time-consuming and complicated. Hence a pseudo-source approach [4] is normally adopted. In this approach, instead of modelling the actual leak source, the leak is modelled from a point or plane downstream of the leak position. This pseudo source is defined such that the flow behaviour further downstream closely resembles that resulting from the actual leak source. In this approach, the release is represented by a sonic jet at atmospheric pressure with the same mass flow rate as the original high-pressure jet. Because of the entrainment into the hydrogen jet and uncertainty of the assumed temperature, this approximation may incur some errors. In the current simulation, the complex under-expanded shock structure is numerically resolved in a small computed domain. The computed results are then used as the inflow conditions for the subsequent hydrogen jet simulation.

The highly under-expanded supersonic jet has previously been investigated by experiments [1-3]. Several numerical studies [3, 5-6] of this kind of flow have also been carried out in the past decades. However, to the best of our knowledge, very few numerical studies were concerned with the highly under-expanded hydrogen jet into an atmospheric environment. This is partly because the very low

density and high sonic speed of hydrogen renders its numerical simulation strongly nonlinear and extremely challenging.

In this study, a highly under-expanded hydrogen jet with a pressure ratio of 105 is numerically studied using two independent CFD codes, namely CFX and KIVA. The KIVA code has been substantially modified by the present authors to facilitate LES calculations [7]. The modified version offers second order accuracy in both time and space. It employs a one-equation sub-grid scale (SGS) turbulence model which solves the SGS kinetic energy equation to allow for more relaxed equilibrium requirement and facilitate high fidelity LES calculation with relatively coarser grids [8].

## 2.0 LES MATHEMATICAL FORMULATION

In LES, the flow field is decomposed into a resolved scale component, which is solved directly, and a sub-grid scale component, which needs to be modelled. To achieve this, a low pass filtering operation is employed. Given a filtering function  $G$ , the spatial filtering operation is defined as:

$$\overline{f(x_i, t)} = \int_{\Omega} G(x_i - z_i) f(z_i, t) dz_i \quad (1)$$

Three kinds of filter are commonly used for LES: Fourier space sharp cut-off filter, Gaussian filter and Box filter. Among these filters, the box filter is the most appropriate choice for finite volume method, which KIVA-3V employs. Accordingly, this study employs the box filter, and  $G$  is given by

$$G = \begin{cases} 1/\Delta V & x_i \in \Delta V \\ 0 & \text{otherwise} \end{cases} \quad (2)$$

In compressible flows, it is convenient to use Favre filtering to avoid the introduction of sub-grid scale terms in the equation of conservation of mass. A Favre-filtered (density weighted) variable is defined as  $\bar{f} = \overline{\mathbf{r}f} / \bar{\mathbf{r}}$ , where  $\bar{\mathbf{p}}$  is the space averaged density. The Favre-filtered equations for compressible flows can then be written as follows:

$$\frac{\partial \bar{\mathbf{r}}}{\partial t} + \nabla \cdot (\bar{\mathbf{r}} \bar{\mathbf{u}}) = 0 \quad (3)$$

$$\frac{\partial \bar{\mathbf{r}} \bar{\mathbf{u}}}{\partial t} + \nabla \cdot (\bar{\mathbf{r}} \bar{\mathbf{u}} \bar{\mathbf{u}}) = -\nabla \bar{p} + \nabla \cdot (\bar{\mathbf{s}} + \mathbf{s}^{sgs}) \quad (4)$$

$$\frac{\partial \bar{\mathbf{r}} \bar{I}}{\partial t} + \nabla \cdot (\bar{\mathbf{r}} \bar{\mathbf{u}} \bar{I}) = -\bar{p} \nabla \bar{\mathbf{u}} + \bar{\mathbf{s}} : \nabla \bar{\mathbf{u}} - \nabla \cdot (\bar{\mathbf{J}} - H^{sgs} + \mathbf{y}^{sgs}) \quad (5)$$

$$\frac{\partial \bar{\mathbf{r}}_m}{\partial t} + \nabla \cdot (\bar{\mathbf{r}}_m \bar{\mathbf{u}}) = \nabla \cdot \left[ \bar{\mathbf{r}} \bar{D} \nabla \left( \frac{\bar{\mathbf{r}}_m}{\bar{\mathbf{r}}} \right) + \mathbf{f}^{sgs} \right] \quad (6)$$

The sub-grid terms in equations (3)-(6) that require closure are:

$$\mathbf{s}^{sgs} = \bar{\mathbf{r}} [\overline{\mathbf{u}\mathbf{u}} - \bar{\mathbf{u}}\bar{\mathbf{u}}], \quad H^{sgs} = \bar{\mathbf{r}} [\overline{I\mathbf{u}} - \bar{I}\bar{\mathbf{u}}] + [\overline{p\mathbf{u}} - \bar{p}\bar{\mathbf{u}}], \quad \mathbf{y}^{sgs} = [\overline{u\mathbf{s}} - \bar{u}\bar{\mathbf{s}}], \quad \mathbf{f}^{sgs} = [\overline{\mathbf{r}_m \mathbf{u}} - \bar{\mathbf{r}}_m \bar{\mathbf{u}}] \quad (7)$$

These terms represent the sub-grid viscous stress tensor, sub-grid heat flux, unresolved viscous work and sub-grid species mass flux respectively. In order to close equations (3)-(6), the one-equation SGS model of Menon [8] is employed to calculate the terms in equation (7). Many LES studies have employed an algebraic eddy viscosity model which uses the grid size as the length scale and the resolved rate-of-strain tensor as the time scale. However, the algebraic eddy viscosity model has some serious limitations. For example, this approach requires equilibrium between turbulent kinetic energy

production and dissipation in small scales, which is possible only if a very high resolution LES grid is employed such that only the dissipation scales are unresolved. By solving the sub-grid kinetic energy, the equilibrium requirement can be relaxed and coarser grid LES is possible. The current simulation involves very large changes of turbulent length scales which would normally demand very fine grid resolution, the choice of this SGS model has to some extent helped to relieve this requirement.

In the one-equation SGS model, the sub-grid stress tensor  $\mathbf{s}_{i,j}^{sgs}$  is expressed as:

$$\mathbf{s}_{ij}^{sgs} = -2\mathbf{n}_t \left[ \bar{S}_{ij} - \bar{S}_{kk} \mathbf{d}_{ij} / 3 \right] + (2/3) \bar{\mathbf{r}} k^{sgs} \mathbf{d}_{ij}. \quad (8)$$

Therefore, to complete the closure for sub-grid stresses, sub-grid eddy viscosity  $\mathbf{n}_t$  and the sub-grid kinetic energy  $k^{sgs}$  need to be modelled. The sub-grid kinetic energy is defined as:

$$k^{sgs} = \left[ \overline{u_k u_k} - \bar{u}_k \bar{u}_k \right] / 2 \quad (9)$$

The evolution equation for sub-grid kinetic energy is given as:

$$\frac{\partial \bar{\mathbf{r}} k^{sgs}}{\partial t} + \nabla \cdot (\bar{\mathbf{r}} \bar{u} k^{sgs}) = P^{sgs} - \bar{\mathbf{r}} \mathbf{e}^{sgs} + \nabla \cdot \left( \bar{\mathbf{r}} \frac{\mathbf{n}_t}{Pr_t} \nabla k^{sgs} \right) \quad (10)$$

The terms,  $P^{sgs}$  and  $\mathbf{e}^{sgs}$  in equation (8) are production and dissipation of sub-grid kinetic energy, respectively. According to Chakravarthy and Menon [9],  $\mathbf{n}_t = 0.067 \sqrt{k^{sgs}} \Delta$ ,  $\mathbf{e}^{sgs} = 0.916 (k^{sgs})^{3/2} / \Delta$  and  $P^{sgs} = -\mathbf{s}^{sgs} : \nabla \bar{\mathbf{u}}$ . Where  $\Delta$  is a length scale taken to be the cubic root of the cell volume. The coefficient  $Pr_t$  is the turbulent Prandtl number and is taken to be 0.9 as in [9].

The sub-grid heat flux  $H^{sgs}$  and the sub-grid species mass flux  $\mathbf{f}^{sgs}$  presented in equation (7) are modelled using the eddy viscosity model as follows:

$$H^{sgs} = \left[ -\bar{\mathbf{r}} \mathbf{n}_t C_p / Pr_t \right] \nabla \bar{T} \quad (11)$$

$$\mathbf{f}_i^{sgs} = \left[ -\bar{\mathbf{r}} \mathbf{n}_t / Sc_t \right] \nabla \left( \frac{\bar{\mathbf{r}}_m}{\bar{\mathbf{r}}} \right) \quad (12)$$

The coefficient  $Sc_t$  is the turbulent Schmidt number which is unity here. Another term that requires modelling is the sub-grid viscous work term,  $\mathbf{y}^{sgs}$ , which is modelled by SGS turbulent energy dissipation rate  $\bar{\mathbf{r}} \mathbf{e}^{sgs}$  in the present study.

### 3.0 NUMERICAL METHODS

The original KIVA-3V [10] solves 3-D unsteady transport equations of a turbulent, chemically reactive mixture of ideal gases, coupled to the equations for a single-component vaporizing fuel spray. The gas phase solution procedure is based on a finite volume method called ALE (Arbitrary Lagrangian-Eulerian) method [11]. Each time the cycle is divided into two phases: a Lagrangian phase and a rezone phase. In the Lagrangian phase the vertices move with the fluid velocity, and there is no convection across cell boundaries. In the rezone phase, the flow field is frozen, the vertices are moved to new user-specified positions, and the flow field is rezoned onto the new computational mesh. This

rezoning is accomplished by convecting material across the boundaries of the computational cells, which are regarded as moving relative to the flow field. In the Lagrangian phase, a variably implicit differencing scheme is used for all the diffusion terms and the terms associated with pressure wave propagation. The coupled implicit equations are solved by a method similar to the SIMPLE algorithm, with individual equations being solved by conjugate residual method [12]. Explicit methods are used to calculate convection in the rezone phase, but the convection calculation can be sub-cycled for an arbitrary number of times, and thus the main computational time step is not restricted by the Courant stability condition of explicit methods. KIVA -3V uses a quasi-second-order upwind (QSOU) scheme for convection. This scheme is monotone and approaches second-order accuracy when convecting smooth profiles. As a whole, the order of accuracy of KIVA -3V numerical schemes is first both in time and space. In order to capture the large eddies, the temporal and spatial accuracy is extremely important in LES. The numerical scheme must be at least second order both in time and space. Considerable modifications were, therefore, carried out to enhance the accuracy of the numerical schemes while modifying the code for LES calculations.

Mittal and Moin [13] have shown that the second-order central differencing with staggered grid provides the energy spectra that are in excellent agreement with its experimental counterpart. Any upwind schemes for convective terms are too dissipative and should therefore be avoided in LES. In our modified LES version of the KIVA code, the second-order Crank-Nicolson scheme has been implemented for the diffusion terms and the terms associated with pressure wave propagation. The two-stage, second-order MacCormack method [14] has been added to solve the convective terms in the rezone phase. For the convection term in the momentum equation, a second-order centred scheme is used to replace the QUOS scheme, which is a quasi-second order upwind scheme and too dissipative for LES. However QUOS scheme remains unchanged for the convection terms in the scalar equations, since the centred scheme may result in overshoots and undershoots in scalar fields for cell Peclet numbers greater than two.

#### 4.0 PROBLEM DESCRIPTION

The computed case in this study is hydrogen release from a high pressure vessel through a circular opening into an atmospheric environment. The pressure and temperature of hydrogen in the vessel are assumed to be 20MPa and 300K, respectively. The diameter of the opening (referred to as D in later discussions) is 0.01m. The leak flow is choked at the exit of the opening, and the exit conditions from the opening can be obtained from the critical condition. Considering the viscous losses on entry to the opening, a discharge coefficient of 0.85 is assumed when determining the exit velocity and flow rate. All the initial data used in this simulation are listed in Table 1.

#### 5.0 RESULTS AND ANALYSIS

Due to the complex shock structures immediate downstream the orifice and the large change of length scale, it is impractical to compute the whole jet region. The numerical calculations were therefore

**Table 1. Initial data in the high-pressure jet simulation**

Vessel pressure (MPa)	20.0	Release temperature (K)	251.0
Vessel temperature (K)	300.0	Release velocity (m/s)	1020.0
Orifice diameter (m)	0.01	Discharge coefficient	0.85
Release pressure (MPa)	10.6		

divided into two stages in the current study. The first stage simulation was carried out using commercial CFD code CFX for the shock structure. The results provided the inflow boundary

conditions for the second stage simulation of the hydrogen jet which was conducted with the LES version of KIVA. The results of both simulations are normalized to the respective inflow conditions and the diameter of the orifice in the analysis.

### 5.1 Simulation of the high under-expansion jet near the orifice

The flow in this region is assumed to be axisymmetric, a 45-degree slice of computed region (50D in diameter and 80D in jet axial direction) was taken. The Reynolds-Averaged Navier-Stokes (RANS) capability of CFX was used with 200,000 unstructured grids. The total energy model was chosen since it takes into account the kinetic energy effects of high speed flows. The k-omega based shear stress turbulence (SST) model was used as it can account for the transport of the turbulent shear stress and is recommended for supersonic jet simulations. In order to capture the shock structures, the high

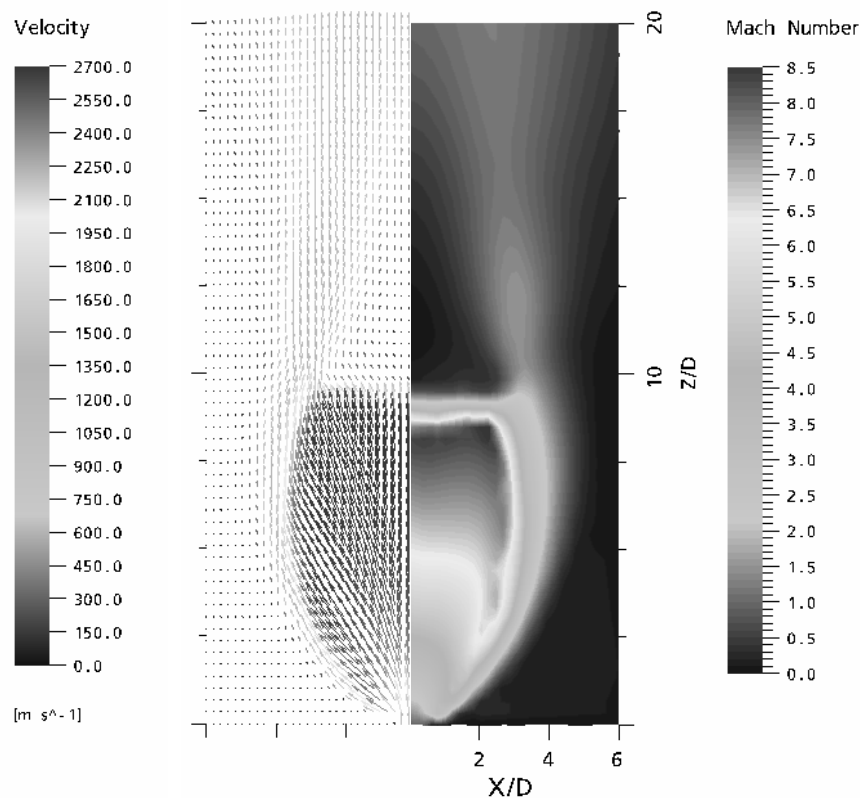


Figure 1. Vector of velocity and contour of Mach number

resolution scheme, which is based on a bounded discretisation technique [15] to represent sharp gradients without numerical oscillations, is used. It is a total variation diminishing (TVD) like discretisation, with a global second order accuracy, which switches to a first order upwind scheme locally to prevent non-physical oscillations. The second order backward Euler scheme was employed to define the discretisation algorithm for the transient term. Fig. 1 shows the contour of predicted Mach number and velocity vector. All the shock structures (barrel shock, Mach disk, deflected shock and slip lines) of the highly under-expanded jet are evident in this plot. The computed Mach disk is seen to be situated at  $z=9.2D$  with a diameter of  $5.6D$ . Very high Mach number value (nearly 9) is found in the region prior to the Mach disk, which could be the double effect of high expansion velocity (2700m/s) and low cooling temperature.

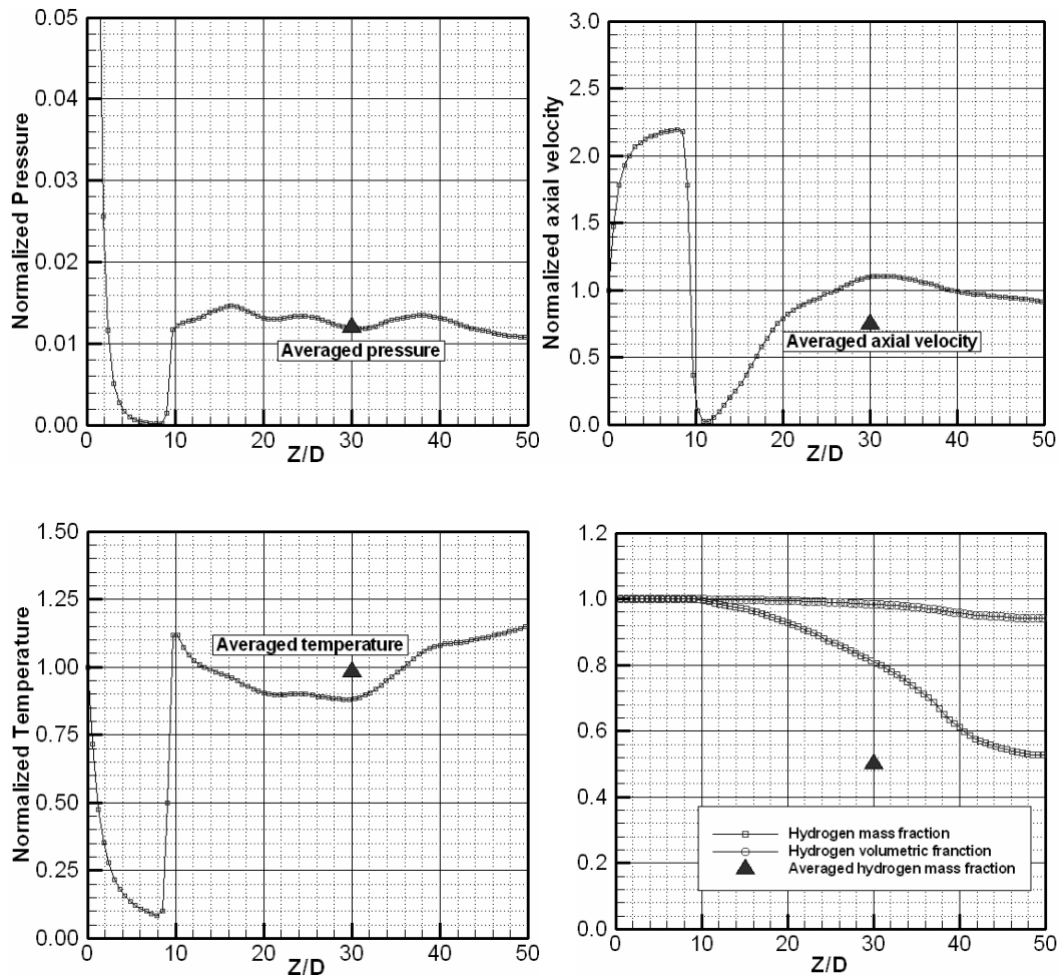


Figure 2. Plots of computed values on the centreline

Fig. 2 shows the centreline values of axial velocity, pressure, temperature, and hydrogen mass/volumetric fractions. Upon exiting the orifice, the hydrogen undergoes strong expansion and cooling. The pressure drops quickly from the critical pressure to a value well below the environmental pressure, and then increases sharply to the environmental pressure while going through the Mach disk. After the Mach disk, the pressure restores to a value a little bit higher above the environmental pressure and then drops to the ambient value again at  $z=30D$ . In line with the change of pressure, the axial velocity accelerates to a maximum value prior to the Mach disk. Immediately downstream the Mach disk, the velocity decelerates to a rather low value and then it accelerates again to a second peak value at  $z=30D$ . After that it decelerates slowly due to the dispersion. Because of the high under-expansion, hydrogen is cooled down to a very low temperature (about 25K), then elevated to a value slightly above the exit temperature immediately behind the Mach disk. Accordingly, the temperature drops gently to a second minimum value at  $z=30D$  again due to the further mild expansion of the jet. After that point, it increases slowly to the environmental temperature. Before  $Z=10D$  (roughly the position of the Mach disk), the hydrogen mass fraction on the centreline remains unity, then decreases gradually downstream the Mach disk. This implies that there is no air entrainment into the centre of the jet prior to the Mach disk due to the high under-expansion and after the Mach disk air entrainment begins to penetrate into the centre of the jet. It is worth noting that the hydrogen volumetric fraction changes little on the centreline, because hydrogen has the lowest molecular weight. From Fig. 2, it can also be seen that  $z=30D$  is a critical height. It marks the end of the shock structure and the near-source expansion of the jet. Above it, the centreline velocity starts to decrease due to momentum exchange

with the outer flow. The flow conditions at this height are therefore considered as the most suitable boundary conditions for the subsequent jet simulation. The axial velocity and hydrogen mass fraction at this height are plotted in Fig. 3. It can be seen that both are very low outside the central core of  $12D$ . The averaged values within this central core, shown as some isolated points in Fig. 2, were hence chosen as the inflow conditions in the subsequent simulation of the jet flow.

Figure 3 also shows that the mass fraction of hydrogen is less than unity even at the centreline implying air entrainment into the jet core. These results suggest that the pseudo-source approach, which neglects air entrainment, may incur some errors when used to provide inflow boundary conditions for such highly under-expanded sonic jet simulations.

## 5.2 Large eddy simulation of the subsequent hydrogen jet

The computational domain in the LES simulation is a box of  $160D \times 160D \times 300D$  as shown schematically in Fig. 4. The mesh contains  $60 \times 60 \times 120$  grid cells clustered near the opening. Inflow boundary condition is specified at the leak source, and a continuative outflow boundary condition is applied to the outlet plane. All the other surfaces are specified as non-slip solid boundaries.

The overall view of the predicted hydrogen jet is shown in Fig. 4 with the iso-surface of instantaneous hydrogen volumetric fraction of 0.3 at  $t=0.05s$ . Highly 3-D structures of the jet are clearly seen in the figure. These structures are also evident in Fig. 5 which shows the contour of instantaneous hydrogen mass density.

Fig. 6 shows the contours of the predicted mean axial velocity and turbulent intensity. Prior to  $Z=50D$ , there is a potential core in the middle of the jet, where the velocity stays almost the same as the exit velocity. The width of the core decreases as the jet moves downstream. After the core diminishes, the velocity drops quickly. This is mainly because of the much lower density value of hydrogen which has two effects here: (1) the momentum exchange following mixing with the air that is constantly entrained into the jet; and (2) the resistance of the upstream air. There exists a high turbulent intensity (0.27) region around  $Z=50-60D$ . Its existence is thought to be due to shear layer instability of a Kelvin-Helmholtz type which produces large scale eddies around the jet and induces instability. Large values of velocity still dominate in this region. The high turbulent intensity enhances the entrainment of air into the hydrogen jet, and further accelerates the decreasing rate of velocity downstream of the region.

Normalized values of main axial velocity, turbulent intensity and hydrogen mass/volumetric fractions along the centreline are plotted in Fig. 7. There is a flat section prior to  $Z=50D$  for both the main axial velocity and hydrogen mass/volumetric fractions. After this point, the dimensionless velocity decreases quickly to 0.2 at  $Z=120D$  due to the intensified air entrainment between  $Z=50D$  and  $Z=120D$  induced by large scale eddies around the shear layer of the jet. From this point on, it reduces more gently. The changing trend of the mass fraction of hydrogen is quite similar to that of the velocity, while the volumetric fraction of hydrogen decreases linearly. The turbulent intensity shows a peak value at  $Z=65D$  on the centreline, which is associated with the shear layer instability and also shown in Fig. 6. The high turbulent intensity enhances the air entrainment into the jet.

Fig. 8 plots normalized values of main axial velocity and hydrogen mass density versus distance to the centreline at different  $Z$  positions. As the jet moves downstream, both the axial velocity and hydrogen mass density show the tendencies of decay in the axial direction and spreading in the direction normal to the centreline due to the exchange of momentum and hydrogen mixing with air in this direction.

The contour of hydrogen volumetric fraction and its flammable range (4% -74%) are plotted in Fig. 9. At the beginning of the jet, there exists a length of high volumetric fraction region (central dark

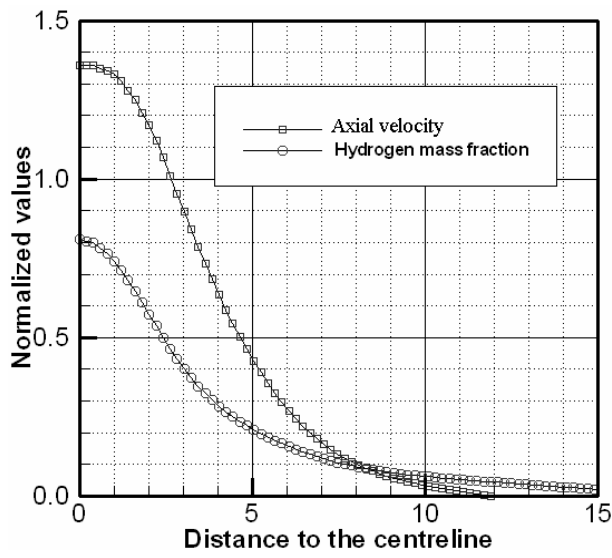


Fig. 3 Plots of axial velocity and hydrogen mass fraction versus distance to the centreline at  $Z=30D$

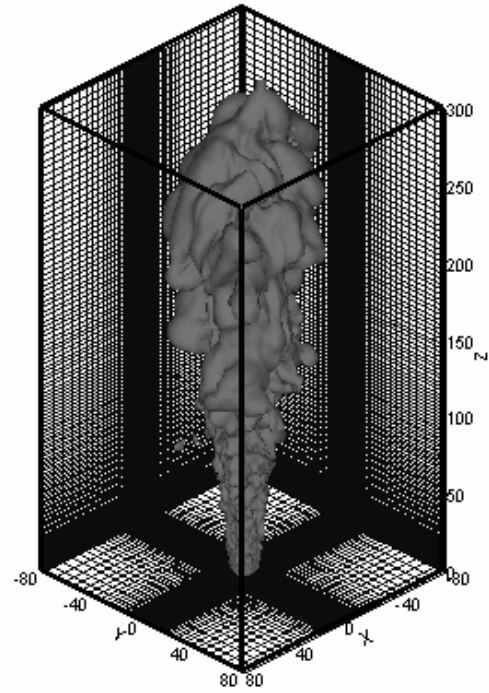


Figure 4. Computed domain and iso-surface of hydrogen volumetric fraction of 0.3 at  $t=0.05s$

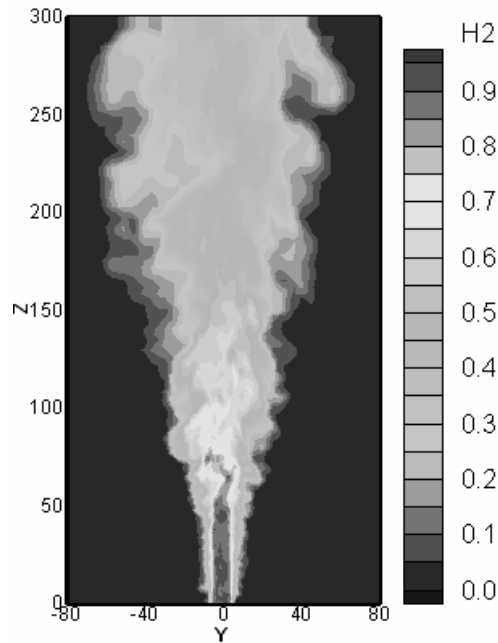


Figure 5. Contours of instantaneous hydrogen mass density normalized to the inflow condition

region) in the jet core extending to a distance about  $125D$ , where the volumetric fraction exceeds the upper flammable limit. Outside this region, there is a large spreading flammable region extending to the jet outlet. Beyond this flammable region, the volumetric fraction is below the lower flammable limit.

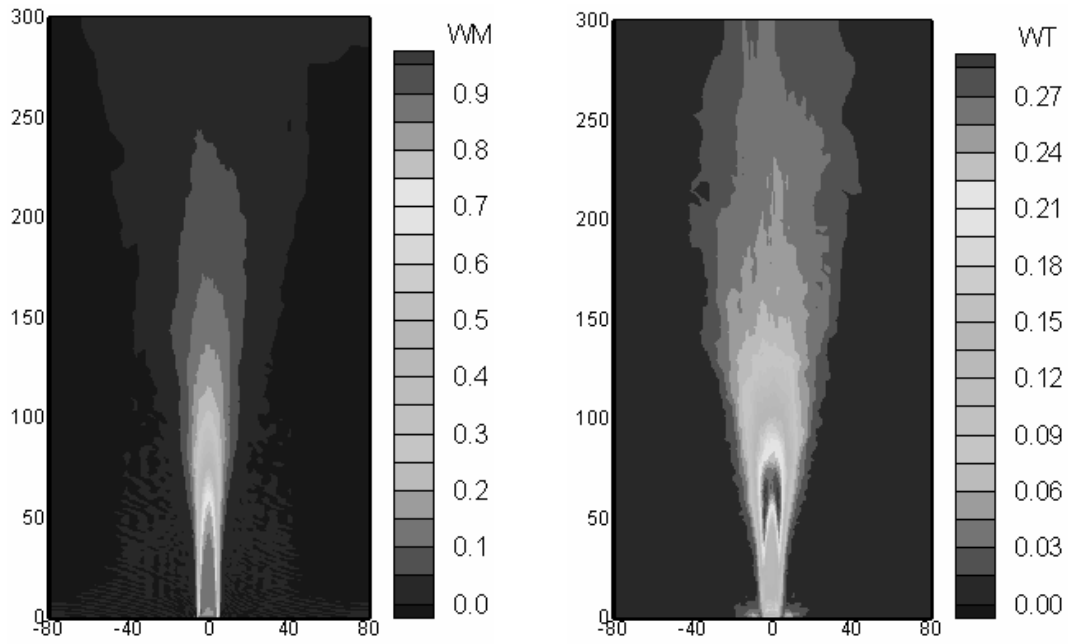


Figure. 6 Contours of time averaged axial velocity (left) and axial turbulent intensity (right) normalized to the inflow condition

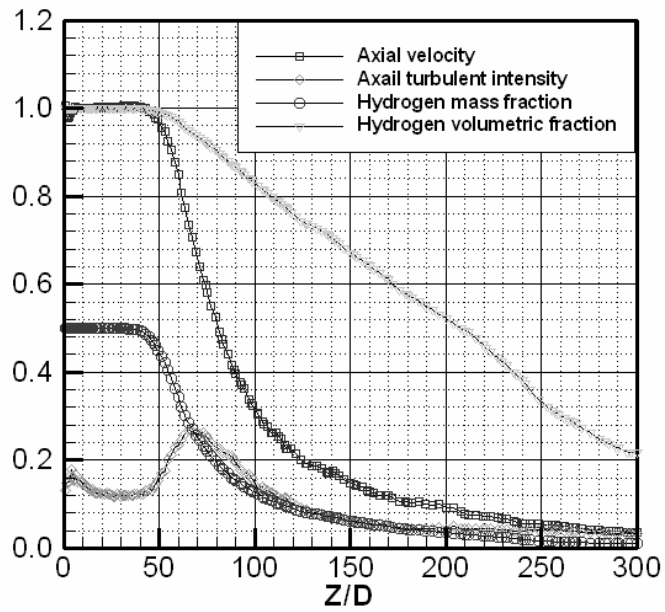


Figure 7. Plots of normalized values of main axial velocity, axial turbulent intensity and hydrogen mass fraction on the centreline

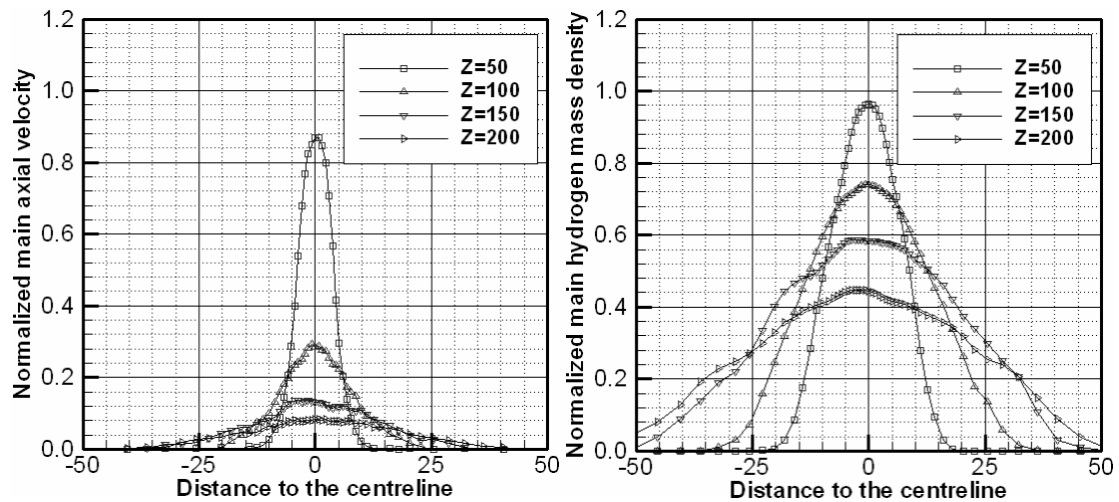


Figure 8. Plots of normalized values of main axial velocity and hydrogen mass density versus distance to the centreline at different Z positions.

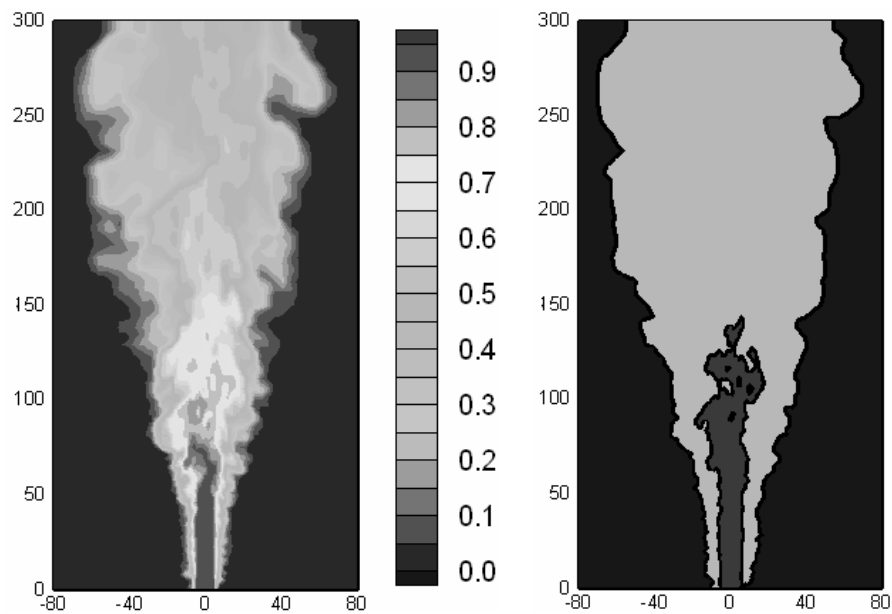


Figure 9 Contours of hydrogen volumetric fraction (left) and flammable range (right) at  $t=0.1s$

## 6.0 SUMMARY

Numerical study of a highly under-expanded hydrogen jet has been carried out by separately considering the shock structure immediately above the release and the subsequent dispersion of the hydrogen jet. For the complex shock structure of the highly under-expanded jet immediately above the jet exit, commercial CFD code CFX was used. The predicted flow pattern and Mach number distribution within the shock structure are in line with previous experimental observation and theoretical analysis of under-expanded sonic jets. Apparent air entrainment is found after these shock structures, implying that the widely used pseudo-source approach may incur some errors for such jet simulations. These results were then used to provide the inflow conditions of a subsequent hydrogen

jet simulation, for which predictions were made using a LES code modified from KIVA-3V. It has been found that downstream the shock structures, there exists a length of a potential core, where both the velocity and hydrogen mass fraction remain almost constant. Subsequently, the velocity decreases quickly due to more air entrainment into the jet. Immediately downstream the potential core, there is a very high turbulent intensity region induced by the shear layer instability of a Kelvin-Helmholtz type. The high turbulent intensity enhances the air entrainment and causes rapid velocity decay.

Although there is no suitable experimental data for quantitative comparison, the predictions provide useful insight about the structure and characteristics of the highly under-expanded jets. The results are also in qualitative agreement with findings from related experiments on other under-expanded jets and theoretical analysis. They also shed light on how hydrogen accidentally released from a high pressure tank will propagate in the air. It shows that a combustible cloud could be formed above the leak source within a very short period of time (about 0.1s), posing great danger during the transportation of hydrogen. Further work is currently under way to consider the effect of ambient wind conditions and simulate the resulting jet flames which could develop following the ignition of such high pressure jets.

## REFERENCES

1. Crist, S. A., Experimental Study of the Shock Structure of a Highly Under-expanded Jet Exhausting from a Sonic Nozzle. *AIAA Student Journal* **3**(2), 1965, 43.
2. Golub, V. V., Development of Shock Wave and Vortex Structures in Unsteady Jets. *Shock Waves* **3**, 1994, pp. 279-285.
3. Ishii, R. and Fujimoto, H., Experimental and Numerical Analysis of Circular Pulse Jets, *J. Fluid Mech.* vol. **392**, 1994, pp. 129-153.
4. Ewan, B. C. R. and Moodie, K., Structure and Velocity Measurements in Under-expanded Jets, *Combust. Sci. and Tech.*, Vol. **45**, 1986, pp.275-288.
5. Cumber, P. S. and Fairweather, M., Predictions of the Structure of Turbulent, Highly Under-expanded Jets, *J. Fluids Engineer*, Vol. **117**/599, 1995.
6. Jugroot, M. and Groth, C. P. T., Numerical Investigation of Ion Transport in Under-expanded Jet Flows, *36th AIAA Thermophysics Conference*, AIAA 2003-4210, 2003.
7. Xu, B. P. and Wen, J. X., Large Eddy Simulation of Plane Impinging Jets, submitted to *International Journal of Heat and Fluid flow*, 2005.
8. Menon, S., Yeung, P. K. and Kim, W. W., Effect of Sub-grid Models on the Computed Interscale Energy Transfer in Isotropic Turbulence. *Computers and Fluids*, **25**(2), 1996, pp.165-180.
9. Chakravarthy, V. K. and Menon. S., Large Eddy Simulations of Turbulent Premixed Flames in the Flamelet Regime. *Combustion Science and Technology*, 162, 2001, pp. 175-222.
10. Amsden, A. A., O'Rourke, P. J. and Butler, T. D., KIVA -2: A Computer Program for Chemically Reactive Flows with Sprays. *Technical report LA -11560-MS*, Los Alamos National Laboratory, May 1989.
11. Hirt, C. W., Amsden, A. A., and Cook, J. L. J., *Comput. Phys.* **14**, 227, 1974.
12. O'Rourke P. J. and Amsden, A. A., Implementation of a Conjugate Residual Iteration in the KIVA Computer Program, *Los Alamos National Laboratory report LA -10849-MS*, 1986.
13. Mittal, R. and Moin, P., Suitability of Upwind-biased Finite Difference Schemes for Large Eddy Simulation of Turbulent Flows. *AIAA J.* **35**, 1997, pp. 1415-1417.
14. MacCormack R. W., The Effect of Viscosity in Hypervelocity Impact Cratering, *AIAA paper*, 1979, pp. 69-354.
15. Barth, T. J. and Jespersen, D. C., The Design and Application of Upwind Schemes on Unstructured Meshes, *AIAA Paper 89-0366*, 1989.
16. T Hayashi and S Watanabe, Hydrogen safety for fuel cell vehicles, Japan Automobile Research Institute, 2003.